CONDENSED MATTER PHYSICS

Superconductivity with twofold symmetry in $Bi_2Te_3/FeTe_{0.55}Se_{0.45}$ heterostructures

Mingyang Chen[1], Xiaoyu Chen[1], Huan Yang[1,2]*, Zengyi Du[1], Hai-Hu Wen[1,2]*

Topological superconductors are an interesting and frontier topic in condensed matter physics. In the superconducting state, an order parameter will be established with the basic or subsidiary symmetry of the crystalline lattice. In doped Bi_2Se_3 or Bi_2Te_3 with a basic threefold symmetry, it was predicted, however, that bulk superconductivity with order parameters of twofold symmetry may exist because of the presence of odd parity. We report the proximity effect–induced superconductivity in the Bi_2Te_3 thin film on top of the iron-based superconductor $FeTe_{0.55}Se_{0.45}$. By using the quasiparticle interference technique, we demonstrate clear evidence of twofold symmetry of the superconducting gap. The gap minimum is along one of the main crystalline axes following the so-called Δ_{4y} notation. This is also accompanied by the elongated vortex shape mapped out by the density of states within the superconducting gap. Our results provide an easily accessible platform for investigating possible topological superconductivity in $Bi_2Te_3/FeTe_{0.55}Se_{0.45}$ heterostructures.

INTRODUCTION

Superconductivity with order parameters of odd parity is highly desired because of the expectation of Majorana fermions and potential applications in quantum computation (*1*, *2*). The topological superconductors are supposed to have order parameters with odd parity, which has now become a hot topic in condensed matter physics. One of the signatures of odd parity is the existence of a superconducting (SC) order parameter with a twofold symmetry, such as p_x- or p_y-wave pairing. However, in reality, it is extremely rare. In some compounds with chemical doping, such as $M_xBi_2Se_3$ (M = Cu, Nb, and Sr), theoretically, it was predicted that the topological SC state may occur (*3*, *4*). Some traces of this long-sought topological superconductivity have been reported together with the observation of the signatures of Majorana fermions or modes (*5*, *6*). Proximity effect is another way to induce possible topological superconductivity (*7*), which has been demonstrated in the Bi_2Se_3 thin film on top of 2*H*-$NbSe_2$ (*8*) and with the possible evidence of a Majorana mode within the vortex core on $Bi_2Te_3/NbSe_2$ heterostructures (*9*). In the doped materials $M_xBi_2Se_3$ (M = Cu, Nb, and Sr), bulk superconductivity was observed (*10*–*12*) and full gaps have been reported on the surface by scanning tunneling microscopy/spectroscopy (STM/STS) measurements (*13*, *14*). Recently, Knight shift of nuclear magnetic resonance (NMR) measurements (*15*) and angle resolved–specific heat (*16*) reveal a twofold feature of superconductivity when the magnetic field rotates within the *ab* plane in $Cu_xBi_2Se_3$. Theoretically, Fu (*17*) did a quantitative assessment by taking into account the spin-orbital coupling and the multi-orbital effect in $M_xBi_2Se_3$ and predicted that it could be possible to have a fully gapped order parameter but with odd parity, namely, a twofold symmetry of the SC order parameter. Furthermore, the *c* axis resistivity also exhibits a twofold symmetry when the applied magnetic field is rotated within the basal plane in $Sr_xBi_2Se_3$ (*18*, *19*). However, to extract the information of gap structure from these data, we inevitably need some models to relate the gap minimum with the crystalline lattice. Here, based on the STM/STS measurements on superconductivity induced by the proximity effect in the Bi_2Te_3 thin film on top of the iron-based superconductor $FeTe_{0.55}Se_{0.45}$, we present the clear evidence of a twofold symmetry of the SC order parameter and pin down the gap form of Δ_{4y} from several candidates (*16*, *17*). We also observe an elongated vortex structure associated with this effect.

[1]National Laboratory of Solid State Microstructures and Department of Physics, Nanjing University, Nanjing 210093, China. [2]Collaborative Innovation Center of Advanced Microstructures, Nanjing University, Nanjing 210093, China.
*Corresponding author. Email: huanyang@nju.edu.cn (H.Y.); hhwen@nju.edu.cn (H.-H.W.)

RESULTS

Scanning tunneling spectra

Single crystals of $FeTe_{0.55}Se_{0.45}$ with a transition temperature T_c of about 13.3 K are used as the substrates. After cleaving the $FeTe_{0.55}Se_{0.45}$ crystal in a high vacuum, we obtain a fresh and clean surface on which we grow the topological insulator Bi_2Te_3 film (see Materials and Methods) by using the molecular beam epitaxy (MBE) technique. As shown in Fig. 1A, the surface topography of $FeTe_{0.55}Se_{0.45}$ shows a square lattice structure. The white and dark atoms were supposed to be the Te and Se atoms, respectively (*20*). The atomically resolved topographic image of the resultant Bi_2Te_3 film with 2-QL (quintuple layer) thickness is shown in Fig. 1B, and it is clear that the top Te-terminal surface has a hexagonal structure. Actually, the hexagonal structure has been formed already for the thin film with 1-QL thickness (see fig. S1). Using a deposition rate of about 0.5 QL/min, we obtain the Bi_2Te_3 thin film with very good connectivity. The thickness changes from place to place; a typical case is shown in Fig. 1C. The height difference between the two sides of a step is about 1 nm, which corresponds to the thickness of a single QL of Bi_2Te_3. The general shape of the spectrum measured on the Bi_2Te_3 film with the local thickness larger than 1 QL is similar to that measured on the $Bi_2Te_3/NbSe_2$ heterostructure (*9*). The exact thickness of the Bi_2Te_3 film in the local area is determined by the features of the tunneling spectra (*9*) with a wide range of bias voltage, which is shown in Fig. 1D. The arrow marking for the kinky position reflects the energy difference of the Dirac point from the Fermi energy for each kind of the film. However, it should be noted that the features of conduction band minimum seem to be absent on the spectra, and the energy position of the kink for the 1-QL film in the present study is very different from that for the 1-QL $Bi_2Te_3/NbSe_2$ heterostructure. In regions with different thicknesses, superconductivity is successfully induced by the proximity effect on the Bi_2Te_3 thin film, which can be observed on the tunneling spectra in the lower-energy range, and the typical spectra are shown in Fig. 1E.

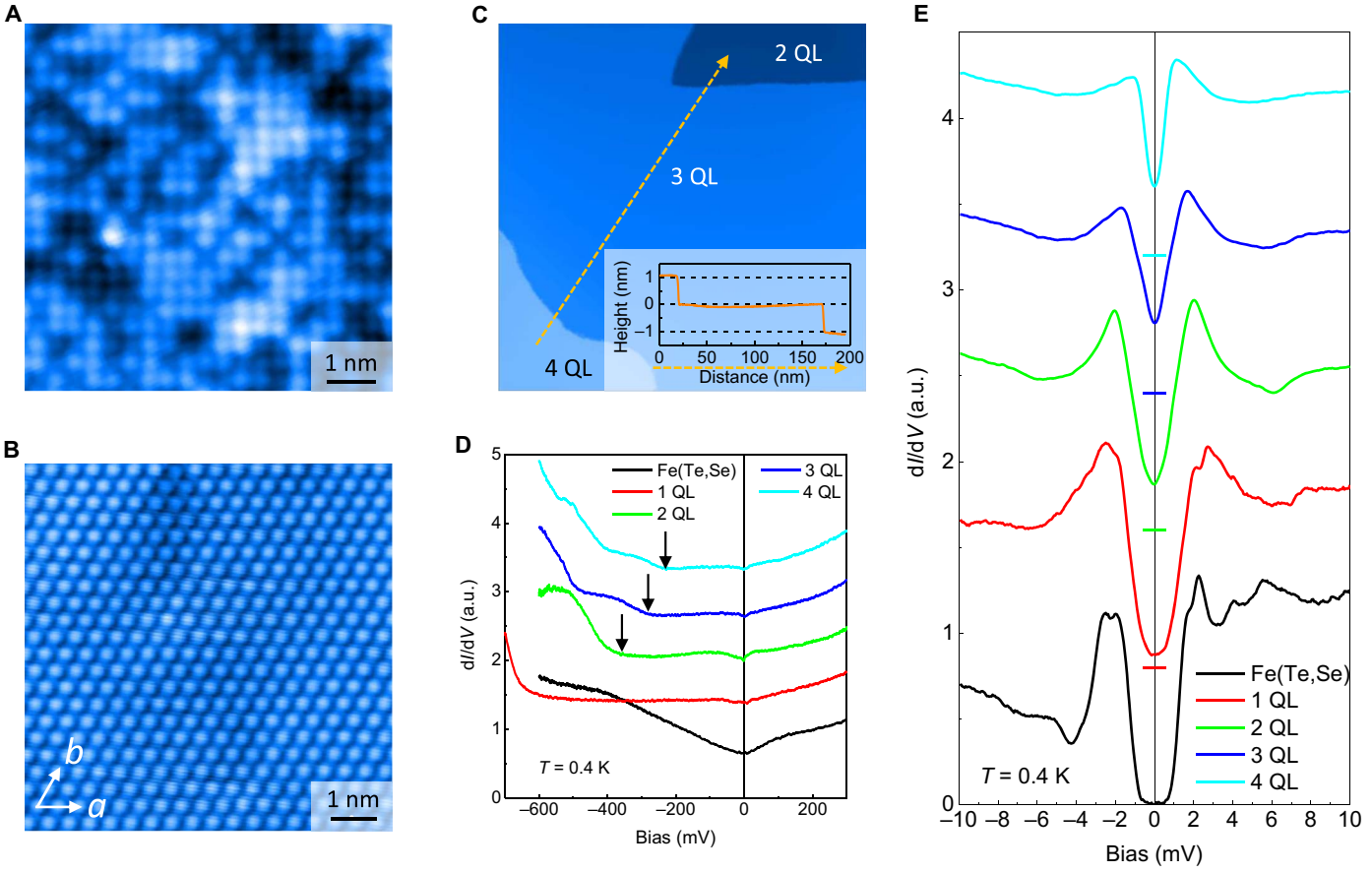

Fig. 1. STM/STS characterization of $Bi_2Te_3/FeTe_{0.55}Se_{0.45}$ heterostructure. (**A** and **B**) Atomically resolved topography (with bias voltage V_{bias} = 10 mV and tunneling current I_t = 200 pA) of the (A) $FeTe_{0.55}Se_{0.45}$ substrate and (B) 2-QL Bi_2Te_3 thin film. The measured lattice constants of the top Te/Se surface on $FeTe_{0.55}Se_{0.45}$ with square lattice and Te surface on Bi_2Te_3 with hexagonal lattice are 3.80 and 4.38 Å, respectively. Using a deposition rate of about 0.5 QL/min, we obtain the Bi_2Te_3 thin film with very good connectivity. The thickness changes from place to place. (**C**) Topographic image (V_{bias} = 2 V, I_t = 10 pA, 150 × 150 nm^2) of Bi_2Te_3 film with different thicknesses. The height difference for each step along the dashed yellow arrowed line is about 1.0 nm, which equals a thickness of 1 QL. (**D**) Typical differential conductance spectra (set-point bias voltage V_{set} = 0.45 V, I_{set} = 300 pA) measured on $FeTe_{0.55}Se_{0.45}$ substrate and Bi_2Te_3 thin films with different thicknesses. The black arrows show the positions of the typical kink features probably from the Dirac point of the Bi_2Te_3 films of different thicknesses. (**E**) Tunneling spectra with SC feature (V_{set} = 10 mV, I_{set} = 50 pA) measured on $FeTe_{0.55}Se_{0.45}$ substrate and 1- to 4-QL $Bi_2Te_3/FeTe_{0.55}Se_{0.45}$. The short horizontal bars with the same color mark the zero differential conductance for each curve. The typical feature of the spectra on the $FeTe_{0.55}Se_{0.45}$ substrate is that one or two pairs of coherence peaks can be observed with peak energies varying from 1.1 to 2.1 meV. The tunneling spectrum measured on 1-QL Bi_2Te_3 also has the trace of coherent peaks of $FeTe_{0.55}Se_{0.45}$. This feature is absent on the 2-QL or thicker Bi_2Te_3 films. a.u., arbitrary units.

The spectra measured on the $FeTe_{0.55}Se_{0.45}$ substrate show a fully gapped feature with some nonuniform shape, which was described in our previous work (*21*). The typical feature of the spectra on the $FeTe_{0.55}Se_{0.45}$ substrate is that one or two pairs of coherence peaks can be observed with peak energies varying from 1.1 to 2.1 meV. As shown in Fig. 1E, the tunneling spectrum measured on 1-QL Bi_2Te_3 has also the trace of such feature of coherent peaks of $FeTe_{0.55}Se_{0.45}$. However, the homogeneity of tunneling spectra becomes much better on Bi_2Te_3 films with a thickness larger than 2 QLs, which is presented in fig. S2. If we assume that the Bi_2Te_3 film is not superconductive, then no gapped feature would be observed on the surface because the thickness of the 2-QL film is about 2 nm, which is beyond the detecting depth of STM. This corroborates that the superconductivity observed here is due to the proximity effect derived from the substrate $FeTe_{0.55}Se_{0.45}$. Meanwhile, by increasing the thickness of the Bi_2Te_3 thin film, the energy difference between two coherent peaks shrinks, and the density of states (DOS) at zero bias also becomes higher. On the surfaces with a thickness of ≥2 QLs, the spectra show a V shape near the Fermi energy. The general shape and the evolution of the spectra with thickness are similar to those of previous results on the $Bi_2Te_3/NbSe_2$ heterostructure (*9*).

Quasiparticle interference

Because the proximity effect–induced superconductivity has been well formed in the 2-QL $Bi_2Te_3/FeTe_{0.55}Se_{0.45}$ heterostructure, it is worth detecting the pairing symmetry of superconductivity. The quasiparticle interference (QPI) technology is a useful tool to detect the SC gap structure (*22*, *23*); hence, we measure the 2-QL $Bi_2Te_3/FeTe_{0.55}Se_{0.45}$ heterostructure to see whether we have the twofold SC gap. The standing waves of the electrons in the QPI measurements contain information in *k* space and are scattered by impurities. They interfere with each other, forming a certain pattern in real space. In our sample, it is generally difficult to find a place with enough impurities because of the good quality of the film. However, successful

QPI measurements were carried out in places with some Te vacancies, and the topography of a typical case is shown in fig. S3A. Figure 2 (A to J) shows the corresponding Fourier-transformed (FT) QPI patterns in q space, with the original QPI shown in fig. S3. If the measuring bias voltage is below 0.5 mV, then no clear intensity can be observed along the hexagon from the FT-QPI. It suggests that the SC gap is nodeless, and the gap minimum, if existing, is larger than 0.5 meV. When the bias voltage is between 1.0 and 1.5 mV, one can find that the intensity of FT-QPI first emerges along one pair of the Γ-K direction marked by the double-arrowed green line in Fig. 2A. This feature can also get support from the real-space QPI images (fig. S3, B to J), as some parallel standing waves are observed. The same feature appears at the negative bias of −1.0 to −1.5 mV. When the bias voltage exceeds 1.5 mV, the other four sides of the hexagon show up gradually. When the bias voltage reaches the SC gap energy of about 2.0 meV, the FT-QPI pattern shows enhanced intensities at two other pairs of Γ-K directions. Another set of data measured with energies up to 4 meV is presented in Fig. 2 (K to O) and fig. S4 as the control experiment. One can see that the FT-QPI at 4.0 mV presented in Fig. 2O shows very clearly the feature of sixfold symmetry, which is consistent with the self-correlation simulation result from a simplified two-dimensional (2D) hexagonal Fermi surface (fig. S5). We refer to this sixfold FT-QPI pattern measured at energies beyond the gap as the normal state one, which is reasonable by considering the crystal structure of Bi_2Te_3. The angle-dependent FT-QPI intensity in fig. S5 is only derived from simulation of joint DOS based on a simplified 2D hexagonal Fermi surface. The results show a

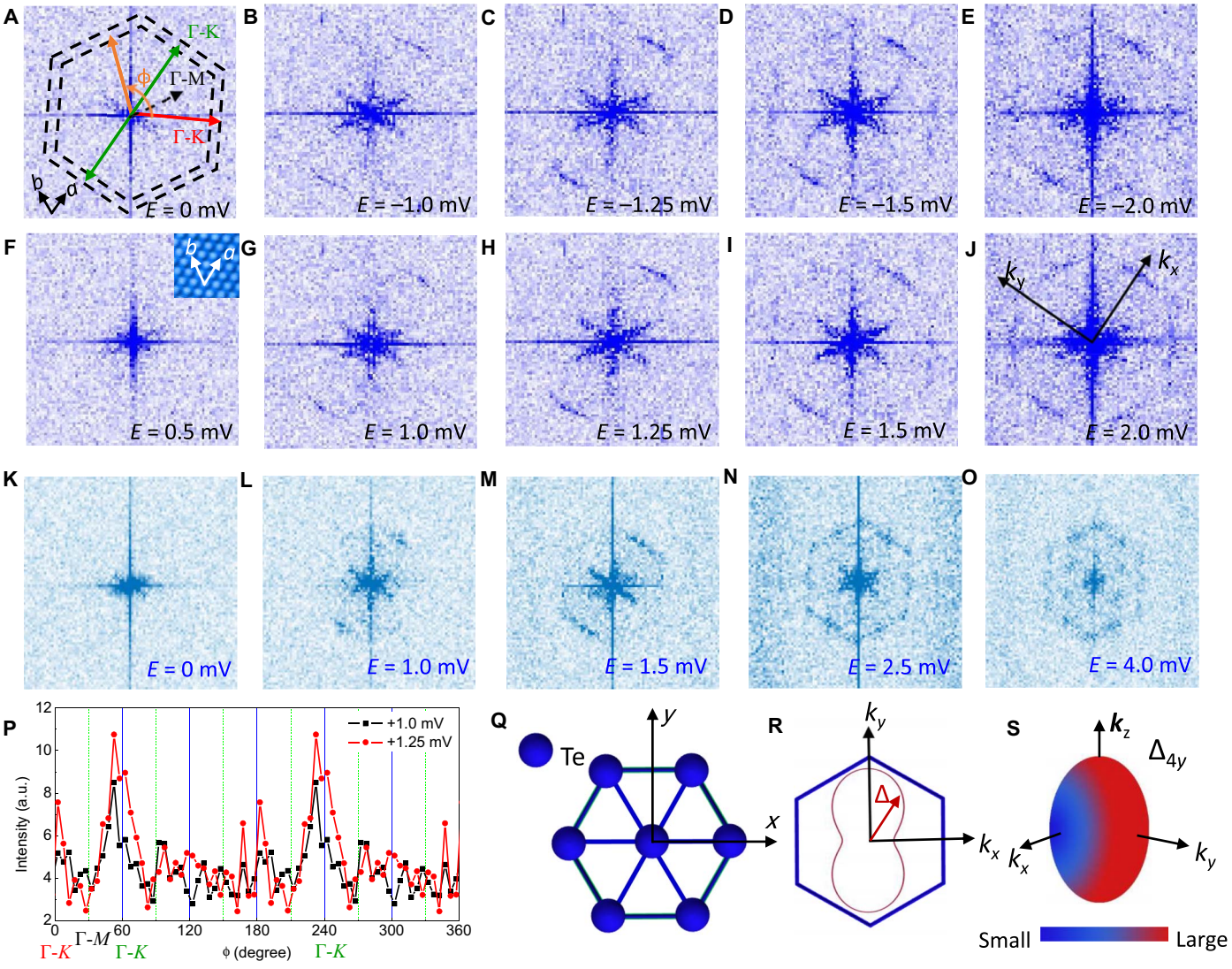

Fig. 2. Twofold SC gap resolved by QPI measurements. (**A** to **J**) The FT-QPI images derived from Fourier transformation to the QPI images at different energies with real-space area of 84 × 84 nm^2 (V_{set} = 10 mV, I_{set} = 50 pA). The inset in (F) shows the topography associated with the QPI measurements. (**K** to **O**) Control experimental FT-QPI results on another 2-QL $Bi_2Te_3/FeTe_{0.55}Se_{0.45}$ heterostructure. The FT-QPI at 4.0 mV presented in (O) shows very clearly the feature of sixfold symmetry. (**P**) The averaged FT-QPI intensity per pixel in the q space of (G) and (H) within the band bounded by the two parallel dashed hexagons in (A) with increment of every 5°. The initial angle of ϕ is defined from one Γ-K direction, as marked by a red arrow in (A). (**Q**) Schematic top view of the Te atom layer of Bi_2Te_3 surface. (**R**) Schematic 2D hexagonal Fermi surface and the resultant angular dependence of the anisotropic SC gap. (**S**) Schematic image of SC gap structures with an oval Fermi surface; the color gives a qualitative distribution of the SC gap.

sixfold symmetry, with the strongest peaks at three pairs of Γ-*K* directions, which is in contrast with the observation of the twofold symmetric FT-QPI in one pair of the Γ-*K* direction at energies below the gap. According to the Bogoliubov theory of DOS in the SC state, a reasonable explanation for the evolution of FT-QPI pattern at energies below 2.0 meV is a twofold SC gap, with gap minima along one pair of the Γ-*K* direction. The twofold symmetry feature is better illustrated in the angular dependence of averaged intensity per pixel, as shown in Fig. 2P and fig. S4G. The intensity peaks near one pair of the opposite Γ-*K* directions (ϕ = 60° and 240°) obviously break the rotation threefold symmetry of the crystal structure. If we compare the result with the Te-terminal surface, then the gap minima locate along one of the crystalline axes. We would argue that the twofold symmetric FT-QPI discovered here is not due to the tip preferential coupling to the anisotropic orbitals (*24*). Theoretically, we have only orbitals with threefold symmetry in the present system. To resolve this issue, we have intentionally measured the Bragg peaks and the QPI in the same area and show the results in fig. S4. The twofold symmetry of the SC gap below 2 meV always appears, as in all other areas, with the gap minimum direction along the *a* axis, while the six Bragg peak intensities are identical or close to each other.

We also tried to use the twofold SC gap functions $\Delta = \Delta_{max}[(1 - x)\cos 2\phi + x]$ to fit the tunneling spectra, and the fitting results are shown in fig. S6. Obviously, the models with only one twofold SC gap can fit the spectra well when they are measured on the Bi_2Te_3 film thicker than 2 QLs. The spectrum measured on the 1-QL Bi_2Te_3/$FeTe_{0.55}Se_{0.45}$ heterostructure (fig. S6A) should be fitted by using the model of two anisotropic gaps, and this may suggest that the spectrum measured on 1-QL Bi_2Te_3/$FeTe_{0.55}Se_{0.45}$ still carries some feature from the $FeTe_{0.55}Se_{0.45}$ substrate. We must emphasize that, just from the fitting, it is impossible to make a decisive judgment whether the gap on the Bi_2Te_3 thin film is two- or fourfold symmetric. Rather, it tells only that the fitting is not inconsistent with the twofold symmetric gap. To illustrate the gap structure from our FT-QPI measurements, in Fig. 2R, we schematically plot the angle-dependent SC gap for the 2-QL Bi_2Te_3 in the same coordinate plane of the contour of the Fermi surface. The gap structure shows a twofold symmetry in *k* space with minimum in one of the Γ-*K* directions. The twofold pairing symmetry has been studied theoretically (*17*), and the direction of the gap minimum found here is consistent with one of the predicted results. According to our experimental results, the notation Δ_{4y} (Fig. 2S) is the only correct pairing symmetry among all the proposals raised by Fu (*17*). This set of experiments has been repeated in three rounds, and all lead to the same observation.

Observation of elongated vortices

The structure of a single vortex in a type II superconductor usually gives rise to the information of the SC gaps (*25*). For example, we can obtain the SC gap Δ by the coherence length extracted from the STM image via $\xi = \hbar v_F/\pi\Delta$, and here, v_F is the Fermi velocity. Because the tunneling spectra look very similar to the ones on the Bi_2Te_3/$NbSe_2$ heterostructure when the film is thicker than 2 QLs, it is quite curious to know whether we have the elongated vortex core because of superconductivity with twofold symmetry. We thus measure the vortex image on the 2-QL Bi_2Te_3/$FeTe_{0.55}Se_{0.45}$ heterostructure and show the main results in Fig. 3. One can see that the vortices are elongated along one of the principal crystalline axes, namely, *a* axis (Fig. 3, A and B), which is very different from the vortex measured on the bare $FeTe_{0.55}Se_{0.45}$ crystal without Bi_2Te_3 (fig. S7B) (*21*). By fitting to the spatial evolution of the zero-bias differential conductance with an exponential decay function, we obtain the anisotropy γ of the vortex, which is about 2.6. The fitting processes are given in

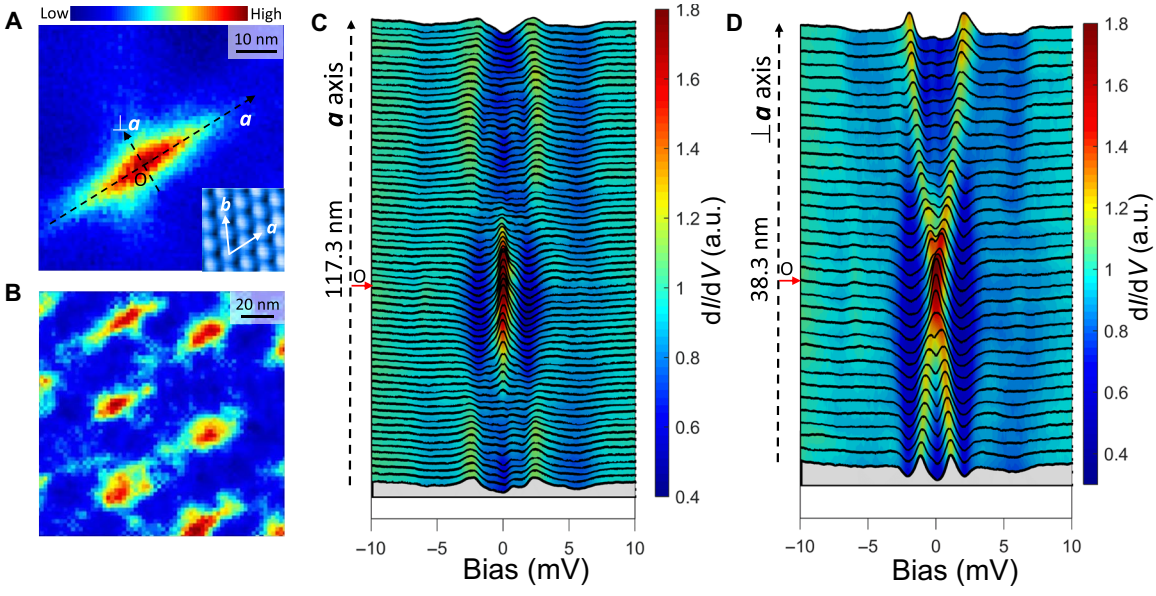

Fig. 3. Vortex image and vortex core states. (**A**) Zero-bias differential conductance map of a single vortex. The inset shows the topography measured near the vortex, and the vortex is elongated along the *a* axis. (**B**) Spectroscopic image of the vortex lattice consisted of elongated vortices measured at zero bias. This elongated vortex shape is very different from that in the bare $FeTe_{0.55}Se_{0.45}$ because of distinct values of Fermi energies. (**C** and **D**) Tunneling spectra measured along *a* axis and perpendicular to *a* axis directions, respectively. The curves marked by the red arrow represent the spectrum measured at the center of the vortex core. It should be noted that the dark dashed lines in (A) only denote the directions of the spectra measurements but do not represent the spatial distance of the measurements. The spectra shown in (C) and (D) are taken along much longer lines than those shown in (A), and the real spatial distance for measuring spectra is given by the vertical dashed arrowed line on the left-hand side of each panel. All data in this figure are taken at T = 0.4 K and B = 0.7 T with V_{set} = 10 mV and I_{set} = 50 pA.

Materials and Methods, and the fitting results are shown in fig. S8. Intuitively, the elongated vortices reflect the in-plane anisotropy of coherence length, which results from the anisotropic SC gap structure in *k* space. The gap minimum direction, which is determined only from the longer coherence length, is consistent with the conclusion from the QPI measurement, that is, along the crystalline *a* axis of the sample. This elongated shape of vortices can be observed in superconductors with twofold symmetric crystal structure (*26*, *27*). However, for Bi_2Te_3, the Fermi velocities along Γ-*K* and Γ-*M* directions are close to each other (*28*, *29*), and obviously, it is difficult to associate these elongated vortices with the Fermi velocity.

We also investigate the vortex-bound states at the center of the vortex core in these elongated vortices on the 2-QL $Bi_2Te_3/FeTe_{0.55}Se_{0.45}$ heterostructure. The anisotropic spatial evolution of the Caroli–de Gennes–Matricon (CdGM) state can reflect the information of the SC gap (*30*). The spatial evolutions of the vortex core state along and perpendicular to the *a* axis are shown in Fig. 3 (C and D). One can find very different vortex-bound state features when the STM tip moves across the elongated vortex. The spectra along the direction with a short vortex core size (that is, perpendicular to the *a* axis) show a central peak at the vortex center and then the peak evolves into two symmetric peaks with strong intensity when moving away from the center. These two peaks will finally merge into the gap edges. This is very similar to the case in a conventional s-wave superconductor with large E_F (*31*). This feature is already very different from the case in the bare $FeTe_{0.55}Se_{0.45}$ crystals in which we observed a round vortex core with the discrete energy levels of CdGM states because of the small Fermi energy (*21*). Thus, we can conclude that the vortex core states on the 2-QL $Bi_2Te_3/FeTe_{0.55}Se_{0.45}$ heterostructure are very different from those on the $FeTe_{0.55}Se_{0.45}$ substrate. We need to emphasize that the superconductivity observed in the $Bi_2Te_3/FeTe_{0.55}Se_{0.45}$ heterostructure is intrinsic, although it comes from the proximity effect. If we go along the elongated direction of the vortex, namely, the *a* axis direction, then the evolution of spectra looks very spectacular. A central peak appears at the core center, stays at zero energy for a distance as long as 40 nm, and then splits into two branches. Compared with the perpendicular direction, the splitting of the peak is weak and less clear, and these two peaks seem not to merge into the gap edges. There is a sharp contrast between the data along two perpendicular directions. At this moment, we still do not have an explicit explanation of these contrasting behaviors along the two perpendicular directions. However, combining the evidence of superconductivity with twofold symmetry shown above, we would propose that this frozen zero-bias conductance peak along the elongated vortex direction may be induced by the complex mixture of a Majorana mode with the CdGM states. The elongated vortex image along the *a* axis strongly suggests that the gap minima are along one of the crystalline lattice directions. When we repeat the measurements at different places, and on different samples (fig. S9), elongated vortices are always observed.

In the following, we demonstrate the twofold superconductivity by measuring the vortex image at different energies. As shown above, the vortices have elongated shapes, as evidenced by the measurements of the zero-bias conductance mapping. It is very interesting to see how the vortex image evolves with the measuring bias energy if the superconductor has a very anisotropic SC gap. We try to image the vortices at different energies in the area whose topography is shown in Fig. 4A. One can find that there is an edge-like dislocation in the upper right corner, which comes probably from the substrate. The elongated vortices can be observed at zero-bias mapping, as shown in Fig. 4B. The elongated direction is again along the *a* axis and has no angular relationship with the direction of the edge-like dislocation. Thus, the elongated vortices or twofold SC gaps are intrinsic properties of the sample and not the effect of extrinsic causes. If the measuring bias voltage is increased but still below the maximum gap of about 2 meV, then the twofold image feature still appears, but the vortex image changes their single elongated shape to a pair of parallel elongated patterns, as shown in Fig. 4 (C to F), which may be originated from the different spatial evolution of the CdGM-bound state peaks along two directions. We are aware that, by increasing the measuring bias voltage from zero to a subgap value in LiFeAs, the vortex image changes from a bright spot to a hollow square with fourfold symmetry (*32*), which may share the same reason as our present case. When the bias voltage is above the SC gap maximum, as shown in Fig. 4 (G and H), the vortex image looks like a roughly isotropic dark disc without a twofold shape. The dark disc feature of the vortices measured at 2.5 mV can be understood by the relative reduction of DOS within a certain region

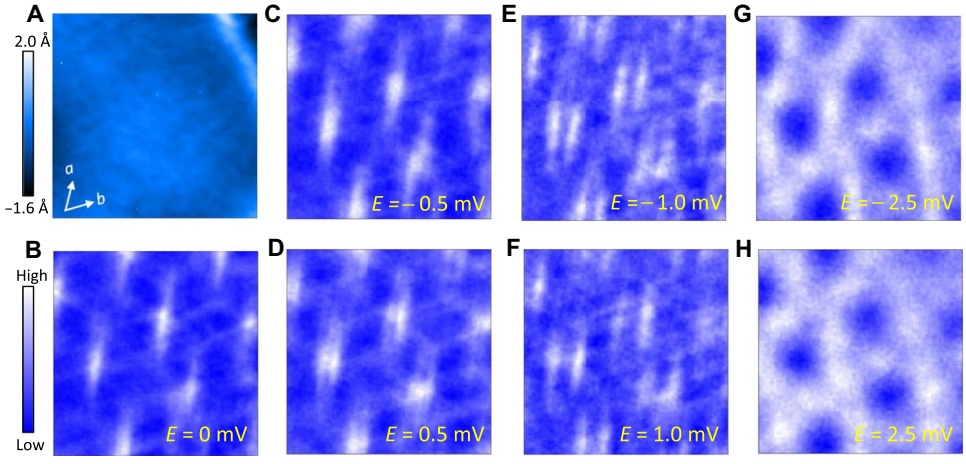

Fig. 4. Energy evolution of vortex image. (**A**) Topography of the view in an area (V_{bias} = 1 V, I_t = 10 pA, 140 × 140 nm^2). (**B** to **H**) Vortex image measured with different bias voltages (V_{set} = 10 mV, I_{set} = 50 pA) at 0.4 K and 0.7 T. Twofold symmetry of the vortex images appears at bias below the gap maximum around 2 meV (B to F). When the measuring voltage is beyond 2 meV (G and H), the vortex images become roughly isotropic dark discs, and the twofold symmetry is absent. This can be understood by the relative reduction of DOS within a certain region in the center compared with that outside that region.

in the center compared with that outside that region. When the energy is larger than the gap maximum, the spatial distribution of DOS along the two characteristic directions does not show a clear difference; hence, it is reasonable that we find such a roughly isotropic image of vortices. This strongly supports the picture that the SC gap has a twofold symmetry. This interesting evolution of vortex images warrants further theoretical investigations.

DISCUSSION

By doing STM/STS measurements and detailed QPI analysis on the 2-QL $Bi_2Te_3/FeTe_{0.55}Se_{0.45}$ heterostructures, we observe the twofold SC gap with the gap minima along one of the principal crystalline axes, which is consistent with the theoretical prediction (*17*). We regard this as a direct observation of the twofold symmetry of superconductivity in the related systems. Because our measurements are done in areas of microscopic scale with atomic resolution, this naturally removes the concern of possible inhomogeneity in bulk samples (*15*, *16*). According to the theory, this twofold symmetry is a natural consequence of the pairing with odd parity of the Δ_{4y} notation.

Concerning the origin of the twofold symmetric superconductivity discovered here, one may argue that it is induced by some extrinsic reasons, such as the interaction between Bi_2Te_3 and the substrate. We would argue that this is unlikely because the FT-QPI intensity at high energy (4 meV) for a 2-QL thin film presented in Fig. 2O shows sixfold symmetry, and the twofold symmetric FT-QPI occurs only within the gap. Furthermore, the vortex image becomes isotropic above the gap energy, while it is twofold symmetric below the gap energy. All these indicate that the SC gap has a twofold symmetry. However, we emphasize that this twofold symmetry of superconductivity is certainly related to and stabilized by the structural details of the interface between the hexagonal and tetragonal structures. Theoretically, the superposition of triangular and rectangular lattices would lead to a shared mirror axis, which, if existing, may provide an explanation for stabilizing the twofold symmetric superconductivity from three possible symmetric orientations.

One interesting issue is why such twofold symmetry of superconductivity and the elongated vortices have not been observed on the $Bi_2Te_3/NbSe_2$ heterostructure (*9*). We argue that this may be attributed to the large scale of coherence length of 2*H*-$NbSe_2$, which transmits the vortex shape on the substrate to the top Bi_2Te_3 surface. Moreover, in the mixed state, the vortex core size in $FeTe_{1-x}Se_x$ is much smaller than that in 2*H*-$NbSe_2$, which makes the area of the proximity effect–induced superconductivity in Bi_2Te_3 much larger in the $Bi_2Te_3/FeTeSe$ case. In this case, the vortex state in Bi_2Te_3 is more dominated by the property of SC Bi_2Te_3, but not from the substrate. The freezing of the central peak of vortex core states along the elongated direction in a rather long distance when moving away from the vortex center may suggest the mixture of a Majorana mode and the CdGM states, which is certainly a very interesting proposal and needs further efforts to verify. Our experimental results bring about deep insight into the understanding of topological superconductivity in this system.

MATERIALS AND METHODS

Sample growth

The $FeTe_{1-x}Se_x$ (with nominal composition of $x = 0.45$) single crystals were grown by self-flux method (*32*). The excessive interstitial Fe atoms were eliminated by annealing the sample at 400°C for 20 hours in O_2 atmosphere followed by quenching in the liquid nitrogen. The $FeTe_{0.55}Se_{0.45}$ samples were cleaved in an ultrahigh vacuum with a base pressure of about 1×10^{-10} torr in the STM chamber. Then, the tunneling spectra were measured before the film growth.

High-quality Bi_2Te_3 films were grown layer by layer on the $FeTe_{0.55}Se_{0.45}$ substrates in a Unisoku MBE chamber, which is connected directly to the STM operation chamber. High-purity Te (99.999%) and Bi (99.999%) were evaporated from the CreaTec effusion cells simultaneously with a flux ratio of about 18:1. The substrate temperature is about 265°C during the film growth, and the film growth rate is about 0.5 QL/min. The process of film growth was monitored by reflection high-energy electron diffraction in the MBE chamber.

STM/STS measurements

The measurements were carried out in a scanning tunneling microscope (USM-1300, Unisoku Co. Ltd.) with ultrahigh vacuum, low temperature, and high magnetic field. Tungsten tips were used for all the STM/STS measurements. A typical lock-in technique was used for the tunneling spectrum measurements with an ac modulation of 0.3 mV and 973.8 Hz. The tunneling spectra were recorded with fixed tip height with some set-point tunneling conditions, and then the *I*-*V* curves and $dI/dV - V$ spectra were measured with such fixed tip height.

Calculation of coherence length

The spatial evolutions of differential conductance along and perpendicular to the *a*-axis direction in Fig. 3A are shown in fig. S8, and the center of the vortex is set as the origin point. Then, we fit the differential conductance $G(r)$ data by an exponential decay law (*33*, *34*) as $G(r) = \exp[-\mathrm{abs}(r)/\xi] + G(\infty)$, where the coherence length ξ and differential conductance far away from the vortex $G(\infty)$ are fitting parameters. The fitting results are also shown in fig. S8, and the resultant coherence length $\xi_{\perp a} = 12.7$ nm, $\xi_{\parallel a} = 33.5$ nm. Hence, the anisotropy of coherence length $\gamma = \xi_{\parallel a}/\xi_{\perp a}$ calculated from the vortex is about 2.6.

Dynes model fitting

We fit the tunneling spectra by Dynes model (*35*) with a single anisotropic SC gap $\Delta(\phi)$ via $I = \int_{-\infty}^{+\infty} d\varepsilon \int_0^{2\pi} d\phi\, [f(\varepsilon) - f(\varepsilon + eV)]\mathrm{Re}\left\{\frac{\varepsilon + eV + i\Gamma}{\sqrt{(\varepsilon + eV + i\Gamma)^2 - \Delta(\phi)^2}}\right\}$. Here, $f(\varepsilon)$ is the Fermi function containing the information of temperature, and Γ is the scattering factor. For the spectrum measured on the 1-QL $Bi_2Te_3/FeTe_{0.55}Se_{0.45}$ heterostructure, one gap is not enough for the fitting, so we use two gaps, that is, a twofold SC gap and a fourfold SC gap, to fit the data. The differential conductivity in the two-gap model is constructed as follows: $G = \alpha dI_1/dV + (1 - \alpha)dI_2/dV$. Here, α is the related spectral weight, and $I_{1(2)}(V)$ is the tunneling current contributed by different SC gaps. In addition, both $I_1(V)$ and $I_2(V)$ can be described by the equation above. A twofold SC gap can be expressed as $\Delta = \Delta_{\max}[1 - \beta(1-\cos 2\phi)]$, while a fourfold one is expressed as $\Delta = \Delta_{\max}[1 - \beta(1 - \cos 4\phi)]$. Here, β is the gap anisotropy. The SC functions and fitting parameters are shown in table S1.

SUPPLEMENTARY MATERIALS

Supplementary material for this article is available at http://advances.sciencemag.org/cgi/content/full/4/6/eaat1084/DC1

fig. S1. Atomically resolved topographies and Fourier transform images of Bi_2Te_3 thin films with thicknesses of 1 and 2 QLs.

fig. S2. Series of tunneling spectra measured on $FeTe_{0.55}Se_{0.45}$ and Bi_2Te_3 thin films.

fig. S3. Real-space QPI patterns at series of energies on the 2-QL $Bi_2Te_3/FeTe_{0.55}Se_{0.45}$ heterostructure.
fig. S4. Control experimental QPI results on the 2-QL $Bi_2Te_3/FeTe_{0.55}Se_{0.45}$ heterostructure.
fig. S5. Simulation of FT-QPI pattern from a 2D hexagonal Fermi surface.
fig. S6. Typical tunneling spectra and theoretical fitting results.
fig. S7. Vortex image on $FeTe_{0.55}Se_{0.45}$ substrate without Bi_2Te_3 film.
fig. S8. The spatial evolution of differential conductance across the elongated vortex.
fig. S9. The control experiments of the elongated vortices.
table S1. SC gap functions and fitting parameters used in the fitting to the tunneling spectra measured on Bi_2Te_3 with different thicknesses at 0.4 K.

REFERENCES AND NOTES

1. X.-L. Qi, S.-C. Zhang, Topological insulators and superconductors. *Rev. Mod. Phys.* **83**, 1057–1110 (2011).
2. Y. Ando, L. Fu, Topological crystalline insulators and topological superconductors: From concepts to materials. *Annu. Rev. Condens. Matter Phys.* **6**, 361–381 (2015).
3. L. Fu, E. Berg, Odd-parity topological superconductors: Theory and application to $Cu_xBi_2Se_3$. *Phys. Rev. Lett.* **105**, 097001 (2010).
4. T. H. Hsieh, L. Fu, Majorana fermions and exotic surface Andreev bound states in topological superconductors: Application to $Cu_xBi_2Se_3$. *Phys. Rev. Lett.* **108**, 107005 (2012).
5. S. Sasaki, M. Kriener, K. Segawa, K. Yada, Y. Tanaka, M. Sato, Y. Ando, Topological superconductivity in $Cu_xBi_2Se_3$. *Phys. Rev. Lett.* **107**, 217001 (2011).
6. S. Nadj-Perge, I. K. Drozdov, J. Li, H. Chen, S. Jeon, J. Seo, A. H. MacDonald, B. A. Bernevig, A. Yazdani, Observation of Majorana fermions in ferromagnetic atomic chains on a superconductor. *Science* **346**, 602–607 (2014).
7. L. Fu, C. L. Kane, Superconducting proximity effect and Majorana fermions at the surface of a topological insulator. *Phys. Rev. Lett.* **100**, 096407 (2008).
8. M.-X. Wang, C. Liu, J.-P. Xu, F. Yang, L. Miao, M.-Y. Yao, C. L. Gao, C. Shen, X. Ma, X. Chen, Z.-A. Xu, Y. Liu, S.-C. Zhang, D. Qian, J.-F. Jia, Q.-K. Xue, The coexistence of superconductivity and topological order in the Bi_2Se_3 thin films. *Science* **336**, 52–55 (2012).
9. J.-P. Xu, M.-X. Wang, Z. L. Liu, J.-F. Ge, X. Yang, C. Liu, Z. A. Xu, D. Guan, C. L. Gao, D. Qian, Y. Liu, Q.-H. Wang, F.-C. Zhang, Q.-K. Xue, J.-F. Jia, Experimental detection of a Majorana mode in the core of a magnetic vortex inside a topological insulator-superconductor $Bi_2Te_3/NbSe_2$ heterostructure. *Phys. Rev. Lett.* **114**, 017001 (2015).
10. Y. S. Hor, A. J. Williams, J. G. Checkelsky, P. Roushan, J. Seo, Q. Xu, H. W. Zandbergen, A. Yazdani, N. P. Ong, R. J. Cava, Superconductivity in $Cu_xBi_2Se_3$ and its implications for pairing in the undoped topological insulator. *Phys. Rev. Lett.* **104**, 057001 (2010).
11. Y. Qiu, K. N. Sanders, J. Dai, J. E. Medvedeva, W. Wu, P. Ghaemi, T. Vojta, Y. S. Hor, Time reversal symmetry breaking superconductivity in topological materials, http://arxiv.org/abs/1512.03519v1 (2015).
12. Z. Liu, X. Yao, J. Shao, M. Zuo, L. Pi, S. Tan, C. J. Zhang, Y. Zhang, Superconductivity with topological surface state in $Sr_xBi_2Se_3$. *J. Am. Chem. Soc.* **137**, 10512–10515 (2015).
13. N. Levy, T. Zhang, J. Ha, F. Sharifi, A. A. Talin, Y. Kuk, J. A. Stroscio, Experimental evidence for *s*-wave pairing symmetry in superconducting $Cu_xBi_2Se_3$ single crystals using a scanning tunneling microscope. *Phys. Rev. Lett.* **110**, 117001 (2013).
14. G. Du, J. Shao, X. Yang, Z. Du, D. Fang, J. Wang, K. Ran, J. Wen, C. Zhang, H. Yang, Y. Zhang, H.-H. Wen, Drive the Dirac electrons into Cooper pairs in $Sr_xBi_2Se_3$. *Nat. Commun.* **8**, 14466 (2017).
15. K. Matano, M. Kriener, K. Segawa, Y. Ando, G.-q. Zheng, Spin-rotation symmetry breaking in the superconducting state of $Cu_xBi_2Se_3$. *Nat. Phys.* **12**, 852–854 (2016).
16. S. Yonezawa, K. Tajiri, S. Nakata, Y. Nagai, Z. Wang, K. Segawa, Y. Ando, Y. Maeno, Thermodynamic evidence for nematic superconductivity in $Cu_xBi_2Se_3$. *Nat. Phys.* **13**, 123–126 (2017).
17. L. Fu, Odd-parity topological superconductor with nematic order: Application to $Cu_xBi_2Se_3$. *Phys. Rev. B* **90**, 100509 (2014).
18. Y. Pan, A. M. Nikitin, G. K. Araizi, Y. K. Huang, Y. Matsushita, T. Naka, A. de Visser, Rotational symmetry breaking in the topological superconductor $Sr_xBi_2Se_3$ probed by upper-critical field experiments. *Sci. Rep.* **6**, 28632 (2016).
19. G. Du, Y. Li, J. Schneeloch, R. D. Zhong, G. Gu, H. Yang, H. Lin, H.-H. Wen, Superconductivity with two-fold symmetry in topological superconductor $Sr_xBi_2Se_3$. *Sci. China Phys. Mech. Astron.* **60**, 037411 (2017).
20. J. E. Hoffman, Spectroscopic scanning tunneling microscopy insights into Fe-based superconductors. *Rep. Prog. Phys.* **74**, 124513 (2011).
21. M. Chen, X. Chen, H. Yang, Z. Du, X. Zhu, E. Wang, H.-H. Wen, Discrete energy levels of Caroli-de Gennes-Matricon states in quantum limit in $FeTe_{0.55}Se_{0.45}$. *Nat. Commun.* **9**, 970 (2018).
22. M. P. Allan, A. W. Rost, A. P. Mackenzie, Y. Xie, J. C. Davis, K. Kihou, C. H. Lee, A. Iyo, H. Eisaki, T.-M. Chuang, Anisotropic energy gaps of iron-based superconductivity from intraband quasiparticle interference in LiFeAs. *Science* **336**, 563–567 (2012).
23. Z. Du, X. Yang, H. Lin, D. Fang, G. Du, J. Xing, H. Yang, X. Zhu, H.-H. Wen, Scrutinizing the double superconducting gaps and strong coupling pairing in $(Li_{1-x}Fe_x)OHFeSe$. *Nat. Commun.* **7**, 10565 (2016).
24. M. J. Lawler, K. Fujita, J. Lee, A. R. Schmidt, Y. Kohsaka, C. K. Kim, H. Eisaki, S. Uchida, J. C. Davis, J. P. Sethna, E.-A. Kim, Intra-unit-cell electronic nematicity of the high-T_c copper-oxide pseudogap states. *Nature* **466**, 347–351 (2010).
25. Y. Wang, P. J. Hirschfeld, I. Vekheter, Theory of quasiparticle vortex bound states in iron-based superconductors: Application to scanning tunneling spectroscopy of LiFeAs. *Phys. Rev. B* **85**, 020506 (2012).
26. C.-L. Song, Y.-L. Wang, P. Cheng, Y.-P. Jiang, W. Li, T. Zhang, Z. Li, K. He, L. Wang, J.-F. Jia, H.-H. Hung, C. Wu, X. Ma, X. Chen, Q.-K. Xue, Direct observation of nodes and twofold symmetry in FeSe Superconductor. *Science* **332**, 1410–1413 (2012).
27. Z. Du, D. Fang, Z. Wang, Y. Li, G. Du, H. Yang, X. Zhu, H.-H. Wen, Anisotropic superconducting gap and elongated vortices with Caroli-de Gennes-Matricon states in the new superconductor $Ta_4Pd_3Te_{16}$. *Sci. Rep.* **5**, 09408 (2015).
28. Y. L. Chen, J. G. Analytis, J.-H. Chu, Z. K. Liu, S.-K. Mo, X. L. Qi, H. J. Zhang, D. H. Lu, X. Dai, Z. Fang, S. C. Zhang, I. R. Fisher, Z. Hussain, Z.-X. Shen, Experimental realization of a three-dimensional topological insulator, Bi_2Te_3. *Science* **325**, 178–181 (2009).
29. T. Zhang, P. Cheng, X. Chen, J.-F. Jia, X. Ma, K. He, L. Wang, H. Zhang, X. Dai, Z. Fang, X. Xie, Q.-K. Xue, Experimental demonstration of topological surface states protected by time-reversal symmetry. *Phys. Rev. Lett.* **103**, 266803 (2009).
30. C. Berthod, I. Maggio-Aprile, J. Bruér, A. Erb, C. Renner, Observation of Caroli–de Gennes–Matricon vortex states in $YBa_2Cu_3O_{7-\delta}$. *Phys. Rev. Lett.* **119**, 237001 (2017).
31. H. F. Hess, R. B. Robinson, J. V. Waszczak, Vortex-core structure observed with a scanning tunneling microscopy. *Phys. Rev. Lett.* **64,** 2711–2714 (1990).
32. T. Hanaguri, K. Kitagawa, K. Matsubayashi, Y. Mazaki, Y. Uwatoko, H. Takagi, Scanning tunneling microscopy/spectroscopy of vortices in LiFeAs. *Phys. Rev. B* **85**, 214505 (2012).
33. Y. Liu, C. T. Lin, A comparative study of $Fe_{1+\delta}Te_{1-x}Se_x$ single crystals grown by Bridgman and self-flux techniques. *J. Supercond. Nov. Magn.* **24**, 183–187 (2011).
34. Y. Yin, M. Zech, T. L. Williams, X. F. Wang, G. Wu, X. H. Chen, J. E. Hoffman, Scanning tunneling spectroscopy and vortex imaging in the iron pnictide superconductor $BaFe_{1.8}Co_{0.2}As_2$. *Phys. Rev. Lett.* **102**, 097002 (2009).
35. R. C. Dynes, V. Narayanamurti, J. P. Garno, Direct measurement of quasiparticle-lifetime broadening in a strong-coupled superconductor. *Phys. Rev. Lett.* **41**, 1509–1512 (1978).

Acknowledgments: We acknowledge useful discussions with Q.-H. Wang. **Funding:** This work was supported by the National Key R&D Program of China (grant no. 2016YFA0300400), the National Natural Science Foundation of China (grant no. 11534005), and the Natural Science Foundation of Jiangsu (grant no. BK20140015). **Author contributions:** The Bi_2Te_3 film growth, low-temperature STS measurements, and analysis were performed by M.C., X.C., H.Y., and H.-H.W. The $FeTe_{0.55}Se_{0.45}$ samples were grown by Z.D. H.Y., M.C., and H.-H.W. contributed to the writing of the paper. H.Y. and H.-H.W. are responsible for the final text. All authors have discussed the results and the interpretations. **Competing interests:** The authors declare that they have no competing interests. **Data and materials availability:** All data needed to evaluate the conclusions of the paper are present in the paper and/or the Supplementary Materials. Additional data related to this paper may be requested from the authors.

Submitted 24 January 2018
Accepted 24 April 2018
Published 8 June 2018
10.1126/sciadv.aat1084

Citation: M. Chen, X. Chen, H. Yang, Z. Du, H.-H. Wen, Superconductivity with twofold symmetry in $Bi_2Te_3/FeTe_{0.55}Se_{0.45}$ heterostructures. *Sci. Adv.* **4**, eaat1084 (2018).